Engineering Applications of Artificial Intelligence 163 (2026) 112905

Contents lists available at ScienceDirect

Engineering Applications of Artificial Intelligence

journal homepage: www.elsevier.com/locate/engappai

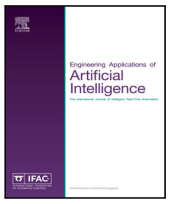

Ensemble modeling of nanoscale thermal drift in high-precision linear axes for photonic integrated circuit testing

Lorenzo Mandelli [a,*], Colin Dankwart [b], Christian Napoli [c]

[a] Department of Engineering in Informatics Automatic and Management, Sapienza University of Rome, Piazzale Aldo Moro 5, Rome, 00144, Italy
[b] Department of Research and Development, ficonTEC Service GmbH, In Finigen 3, Achim, 28832, Lower Saxony, Germany
[c] Dpt. of Computational Intelligence, Czestochowa University of Technology, ul. Dabrowskiego 69, Czestochowa, 42-201, Poland

ARTICLE INFO

Keywords:
Nanoscale thermal drift
Data driven modeling
Auto weighted voting ensemble modeling
Photonic integrated circuits testing
Dynamic-range thermal features
Intelligent manufacturing

ABSTRACT

The consistently growing demand for robust automated assembly, testing and packaging of photonic integrated circuits, is increasingly oriented towards high volume and continuously sets new challenges to overcome concerning throughput and cost-efficiency. Among the predominant positioning error sources in high-precision robots used in this market, thermally induced position drift is often a major cause of deviation from operational conditions required to meet this demand. Environmental temperature fluctuations and the excess heat generated by the machine itself, can induce position drifts upwards of 100 nanometer per minute that prevent axis systems from meeting positional precision and repeatability required for optimal functioning, eventually imposing the integration of expensive temperature control systems and hardware changes that minimize the impact of thermally induced errors. In this paper, a data driven approach for modeling the temperature induced position drift and its dependency on the underlying temperature gradients is proposed. We suggest a formulation that allows to identify temperature gradients calculated over time windows of variable, optimal widths, that capture longer and shorter term drift components, introducing the concept of *dynamic-range thermal features*. By extracting several features from a single sensor, it is possible to reduce the amount of sensors required for an accurate reconstruction, resulting in significant hardware simplification and robustness towards variable field conditions. Additionally, an auto-weighted voting regression algorithm is proposed to separate the modeling of transient states from static and quasi-static states; an auto-regressive model of the position gradients with exogenous temperature gradients and a linear regression model of temperature gradients, are trained independently and combined in a voting ensemble paradigm. Experimental results are presented to quantify the effects of a model-based position compensation schema. Under high ambient temperature fluctuations of ± 1 degree Celsius, position drift is reduced from 23 nanometer per minute to 8.7 nanometer per minute root mean squared error. The proposed approach is validated in the context of photonic die testing with a heated chuck hosting the chip. Correction actions reduce thermal effects from 53 nanometer per minute to 10 nanometer per minute root mean squared error under normal working conditions. Finally, effects on the optical coupling loss and the system settle time are evaluated. Optical losses over 5 min measurement time of components with mode field diameters under 3 micrometer, can be reduced below 0.05 decibel for chuck temperatures up to 50 degree Celsius and a two-sided optical alignment; for chuck temperatures above 50 degree Celsius, the settle time to reach sufficient stability for optical measurements is reduced from 82 min to 32 min.

1. Introduction

The reduction of thermal errors is critical in all applications that require high-precision measurements and sensing (Yang et al., 2019; Stejskal et al., 2017; Wu et al., 2021) as well as precision manufacturing processes (Jedrzejewski et al., 2008). A rich body of research in the literature investigates thermal effects' impact on the accuracy of 3 and 5 axes high-precision milling machinery (Vogl et al., 2023) and for large manipulators with several degrees of freedom (DOF) (Sigron et al., 2023). The main focus of those works is on thermal errors induced by frictional heat of milling, cutting and lathing operations as well as thermal errors produced by environmental temperature changes and manipulators' joints self-heating (Li and Zhao, 2016). Those effects generate position errors in the range of tens to hundreds of μm in the

* Corresponding author.
E-mail address: mandelli@diag.uniroma1.it (L. Mandelli).

https://doi.org/10.1016/j.engappai.2025.112905
Received 16 January 2025; Received in revised form 13 October 2025; Accepted 20 October 2025
Available online 29 October 2025

investigated systems. Fewer works have been conducted on the topic of nanometer scale thermal expansion of high-precision machines employed for assembly, testing and packaging of microscopic components such as microelectronics and photonic circuits. In the proposed study, Photonic Integrated Circuits (PICs) manufacturing systems' thermal behavior is investigated with a particular attention towards industrial use scenarios. The need for high-performance optoelectronic devices is largely driven by an increased demand for higher data-transfer rates across communication networks, and for low-cost sensors to support the internet-of-things and point-of-care medical diagnosis (Lee et al., 2016). In response to the increasing quality requirement of integrated electronic circuits (EICs) and integrated photonic circuits like Silicon Nitride (SiN), Indium Phosphide (InP) and Silicon Photonics (SiPh), impressive progress in advanced motion control of precision mechatronics has followed Evers et al. (2018). Compared to EICs, assembly, packaging and testing of PICs require specific methods and processes, which feasibility strongly depends on very high stability and repeatability requirements. Popular material choices for PICs like InP and SiPh employ feature sizes below the wavelength of light (Klamkin et al., 2018), thus increasing integration capabilities at the cost of production processes that requires realizing motion with nanoscale precision (Leijtens et al., 2020); thermal errors in the range of tens to hundreds of nanometers are critical and prevent from meeting the constantly increasing repeatability requirements dictated by the field. For this reason, industrial systems often require being qualified and calibrated with high precision measurement devices, to meet position stability and repeatability specifications. Position measurements are performed using laser interferometers with resolution in single digit nanometer range, rotations are measured using autocollimators with resolution of 0.1 arcsec and temperatures are collected with positive or negative temperature coefficients sensors (PTC, NTC) (Lubrano and Clavel, 2008). Due to limitations of hardware related solutions for thermal stabilization and thermal drift, software alternatives for estimation and compensation of temperature dependent errors, have already been proposed and extensively discussed in existing works. In Ramesh et al. (2000) the authors review the work carried out over a decade of research. Predictive compensation models can be employed to reduce thermally induced errors and achieve better precision. Several proposed error compensation solutions integrate Machine Learning (ML) (Tu and Peng, 2020) and Deep Learning (DL) models (Tan et al., 2003; Ngoc et al., 2023) in position and orientation errors compensation schemes based on supervised online learning (Mayr et al., 2018; Blaser et al., 2017). Proposed methodologies rely on high-end measurement systems, as well as a high number of temperature sensors, thus being intrinsically limited to scenarios of use where a measurement of the drift is possible during regular operation of the system and remain strongly dependent on the measurements' precision. Although capabilities of modeling nanometer scale thermal drift have been demonstrated, the integration complexity of the proposed solutions do not currently meet the scalability requirements demanded in the field of high-precision manufacturing. Two main limiting factors are identified, being the integration and accessibility of measurement systems for position and rotations tracking and the number and placement of required temperature sensors. In the following paper, both limitations are considered. To overcome this shortcomings, a methodology that combines accessible position measurements and optimal thermal features extracted from few temperature measurements, is proposed to simplify the underlying model complexity and meet robustness, integration and scalability requirements of industrial grade applications. The contribution of this work can be summarized in two points:

(i) It is proposed a linear reconstruction of thermally induced position drift, through *dynamic-range thermal features*, being a close-set of past states of the axis system's measured temperature gradients convolved with windowed functions of variable widths. Multiple optimal widths are identified by analyzing the zero crossings of a successive difference's Fourier transform term. Dynamic-range thermal features

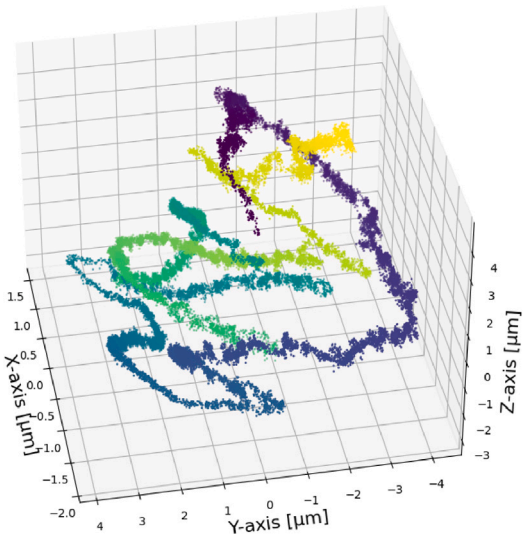

Fig. 1. Position measurements of 3 linear axes (X,Y,Z-axis) employed in PICs manufacturing. Data displayed is collected over the course of 48 h. Temporal information is encoded in the color intensity of the scatter plot. The total position drift is variable along the axes in analysis, ranging from c.a 4 µm to 10 µm.

are used to simplify the learning problem by reducing the modeling complexity, thus improving integrability and scalability requirements. (ii) It is proposed a formulation based on modeling different thermal drift states by separate, distinct learning algorithms that exploit exogenous and endogenous features of the system. Position gradients are considered as a metric of the thermal drift. Sequences of position gradients are considered endogenous features of the system and used to model motion driven effects. Dynamic-range thermal features are considered exogenous features of the system and used to model temperature induced effects. Separate models instances are used within an auto-weighted voting ensemble model. The voting paradigm allows generalizing thermally induced position drift under variably stable thermal conditions, being stable, quasi-stable and transient states, from both positional and thermal information, thus introducing intrinsic robustness towards variable field conditions and partial lost of observability due to sensor faults and inaccessible position measurements (see Fig. 1).

The proposed methodology is finally validated in the context of PICs testing under unstable thermal conditions; the optical signal stability specifications are used to evaluate model-based compensation actions. It is demonstrated that the optical loss stability can be improved beyond limitations imposed by the test conditions. The rest of this article is organized as follows:

In Section 2 relevant research works are discussed and compared within the context of this study and with respect to the introduced research gaps. In Section 3 the methodology is laid out with careful attention to formally introducing the derivation of dynamic-range thermal features, describing the data collection set up and procedures as well as the modeling choices. In Section 4 proof of concept experimental results are gathered from data collected with a set-up composed by a linear axis system with 3DOF capable of realizing 39 nm resolution motion, 4 PTC temperature sensors, and a camera-based vision system which achieves 12 nm standstill repeatability position measurements. In Section 5 the proposed approach is validated within the context of PICs testing with particular attention towards actual process requirements and how those are affected by thermal drift and a correction mechanism. A double side alignment is performed with two 6DOF motion systems under variable thermal conditions. In Section 6 considerations about practical use cases, integrability, scalability and limitations of

the proposed solution are discussed. The Section 7 summarizes the conclusions. In Appendix fundamental linear properties of the heat kernel are discussed, frame theory is introduced to reconstruct thermal expansion from impulse response functions and properties of successive differences are discussed to derive windowed linear terms with optimal width. Finally the contribution of multiple DOF position error to the optical loss during measurements of a PIC is discussed.

2. Literature review

Overall, data driven approaches in the current literature can be categorized by the state of the system that they have been optimized for, in terms of the system stability, the general modeling approach and the type of features that are extracted from the data. In the following we discuss 3 general groups of approaches proposed in the literature, their respective advantages and disadvantages and how the respective system state is defined in the context of this work:

Stable states: static modeling with short-term exogenous features. This is defined as static drift behavior. Under static working conditions, the heat transfer into a body, the transfer between bodies and the thermal expansion law are expected to be linear processes (Drebushchak, 2020; Pluta and Hryniewicz, 2012). When static working conditions are met, observations of temperature readings at a fixed point in time can be used to model the steady state drift of the system. Those are considered exogenous features of the system containing short-term thermal information that are used within the context of static modeling. Static modeling approaches aim at generalizing position drift from purely exogenous features of the system that capture the current thermal state of the machine but not its evolution. An early example of thermal drift static modeling is achieved through a multi regression approach (MRA) presented in Chen et al. (1996). Several independent variables are identified over many thermocouples positioned in the modeled environment and a step-wise regression is used to selectively discard independent variable which do not contribute to increase the model performance. A second-order regression model, which included the first and second-order terms of temperature rise and the interaction terms between any two temperature measurements, is used to solve the regression problem. Static models often tend to have scarce generalization power and can be unreliable when working conditions are different from the tested conditions. Moreover, static models require employing high number of temperature sensors to introduce redundancy (Vocetka et al., 2021; Gao et al., 2023; Li and Zhao, 2016) and achieve accurate and reliable predictions. Stable states are identified within static working conditions, hence when no motion is taking place, and temperature variations induce absolute positional drift below $30\,\mathrm{nm/min}$ within the context of this work.

Quasi-stable states: static modeling with endogenous and short-term exogenous features. Within a framework where motion and continuous control actions are involved, thermoelastic processes induced by quasi-static coupled contact between moving bodies of the machine, like the motors coil and the ball bearing sliders, are identified as a source of non-linearity in the drift behavior (Zagrodzki et al., 2001). Those effects are naturally amplified when sliding frictional contact occurs and are referred in this work as the quasi-static component of drift behavior. In Barber (2016) the effects of bodies sliding against each other are investigated; frictional heat is generated and the resulting thermoelastic deformation alters the contact pressure distribution, causing localization of load and heat generation and hence to hot spots at the sliding interface. Similarly, the authors of Attia and Kops (1979) perform an analysis of the heat transfer across the joints of machine tool structures and a non-linear thermoelastic behavior is established, being caused by two distinctive factors. Firstly, the material nonlinearity causes the stiffness of the surface asperities to take a nonlinear, load-dependent form. The second factor is the nonlinearity resulting from the thermoelastic behavior of contacting elements, which experience a closed-loop interaction between the thermal field and the thermal deformation of structural elements in contact. As a consequence of this phenomenon, the localized behavior of the drift is expected to have a non-linear component that is position dependent. Non-linear components of the drift cannot be generalized only from static temperature observations, especially under the assumption of non-reproducible working conditions. Continuous position measurements, referred to as endogenous features of the system, are required to model the quasi-static drift behavior and increase overall precision and robustness of a model. Authors of Lubrano and Clavel (2010) have incorporated external position measurements in the modeling problem introducing a parametric model, which parameters separate the geometrical error contribution from the thermal induced error component, demonstrating it is possible to achieve $10\,\mathrm{nm}$ precision by compensation. Quasi stable states are identified when the absolute positional drift is measured above $30\,\mathrm{nm/min}$ and below $80\,\mathrm{nm/min}$ within the context of this work.

Transient states: dynamic modeling with endogenous and short-term exogenous features. Differently from quasi-stable and stable states, transient states are induced by rapid temperature changes in the work space, strong self-heating due to bodies' sliding frictional contact when particular motion and poses are executed or by a combination of both scenarios. Thus, as in quasi-static working conditions, it is required a modeling strategy that exploits both exogenous and endogenous features of the system to increase the precision and robustness of predictions. The short-term nature of features extracted from a reduced number of observations, do not capture the dynamical thermal behavior of the system. Thermal features, extracted with a fixed window size, under represent faster and slower components of the drift that are not represented by the chosen window size for the position drift calculation. For these reasons, it is required a dynamic modeling approach that takes in consideration the past and forecasted temperature and position states of the system, by combining dynamic exogenous and endogenous features of the system, thus offering better robustness when non-reproducible working conditions are faced. To overcome the limitations of a purely static modeling approach, an early instance of a dynamic model is proposed in Yang and Ni (2003). The authors identify thermal errors to do not be determined only by the current thermal environment but also influenced by the proceeding thermal status of the machine. This characteristic is called the pseudo-hysteresis effect in the paper, and it is identified to be the major factor causing poor robustness of the conventional static thermal error model. A better reconstruction of the position drift is therefore possible from temperature features calculated over time windows with variable length. In Tan et al. (2003), Kim et al. (2011) and Tu and Peng (2020) dynamic modeling of thermally induced errors is achieved through state space modeling, auto-regressive models (AR), auto-regressive models with moving average (ARMA) as well as auto-regressive models with integrated moving average (ARIMA). Finally, modeling approaches that rely on both endogenous and exogenous features such as AR, ARMA and ARIMA with endogenous and exogenous inputs (ARX, ARMAX, ARIMAX) have been proven robust towards variable conditions as well as ease the integration in embedded systems. Transient states are identified when absolute positional drift over $5\,\mathrm{min}$ is calculated to be above $80\,\mathrm{nm/min}$ within the context of this work.

A methodology based on reconstruction of position drift from thermal features that contains long and short-term components of the drift (i.e. calculated over variable window width) can be expected to increase the model capabilities. However, in order to generalize position drift information from a reduced set of temperature sensors, the overall model complexity shall increase; it is clear that calculating long-term signal components requires larger amounts or higher quality data. This can be achieved by either increasing the number or precision of temperature sensors, both of which come at technical and financial cost. Due to the scarce robustness of modeling approaches based on short-term thermal features, existing solutions for calibration and

Table 1
Comparison of related works in thermal error modeling and compensation of high-precision robotic systems.

Paper	Methodology	Problem focus	Main limitations
Yang and Ni (2003)	Stepwise regression for thermal calibration via inverse geometric model	Modeling thermoelastic process as a dynamic system	Only short term thermal effects are recorded (sampling interval of 30 s) imposing placing the sensor as close as possible to heat sources
Lubrano and Clavel (2008, 2010)	Linear Output Error (OE)	Separate the geometrical error contribution from the thermal induced error component	Require autocollimators and interferometers to measure position changes over time
Kim et al. (2011)	State space modeling	Investigate dynamic modeling (ARX, OE, Box Jenkins) approaches through system identification theory	The model identified trades prediction accuracy for robustness
Li and Zhao (2016)	Calibration of robot kinematic parameters through finite element theory	Compensation of thermal deformation induce by the ambient temperature changes and self-heating effect	The problem complexity explodes when considering all kinematic parameters and a larger spectrum of working condition
Tu and Peng (2020)	Auto-regressive moving average (ARMA) technology	Modeling transient and steady state drifting behaviors with linear and nonlinear AR models (ARMA) and exogenous inputs (NARX)	Over-reliance on the measurements and reproducibility of the observed conditions (minimum difference filter (MDF) to suppress the noise disturbance)
Vocetka et al. (2021)	Matlab regression learner	Improve Tool Center Position (TCP) repeatability by compensation of position errors produced by joints self-heating	High number of temperature sensors to introduce redundancy
Proposed work	Auto-weighted voting regression with dynamic-range thermal features	Identification of dynamic-range thermal features that capture longer and shorter term drift components and separate the modeling of different stability states through auto-weighted voting	Full capabilities of proposed approach are limited by the observability of the system position over time

non-geometric error compensation of high-precision industrial robots presented in the field rely on high-end measurement systems, such as interferometers (Lubrano and Clavel, 2010) and laser trackers (Li and Zhao, 2016), as well as a high number of temperature sensors (Vocetka et al., 2021). Methodologies based on purely endogenous features as well as approaches employing static and dynamic modeling of short-term temperature information, are limited to scenarios where a measurement of the drift is possible during regular operation of the system and remain strongly dependent on the measurements' precision and redundancy of temperature measurements. Proposed dynamic-range thermal features contain information of past and present thermal states of the system that are needed for the reconstruction problem, thus permitting to simplify the overall implementation by reducing the amount of sensors required; historical position data and dynamic-range thermal features are used to separate the regression of steady and transient position drift's dynamics through ensemble modeling, thus increasing the overall prediction precision and robustness of the solution. A comparative overview of existing key works and the proposed approach is reported in Table 1 to highlight how the current work advances the existing research gaps.

3. Methodology: Thermal drift modeling

In this section, considerations on the properties of the heat equations and the heat kernel (discussed in Appendix A.1) are used to frame the problem of predicting the time dependent position of a fixed point on an axis system, through the time dependent temperature measurements on its surface. A linear modeling approach is derived through a formulation based on reconstructing successive differences of the thermal drift impulse response by frames (discussed in Appendix A.2) instead of bases of orthogonal vectors. This allows a direct application of known properties of the solution as constraints, so to reduce complexity and increase robustness and accuracy of the predictions. Finally, a windowed linear function with window widths that share some of the zero crossings of the successive difference's Fourier transform term is considered to be adequate to impose known boundary conditions on the reconstructed impulse responses and therefore used for the definition of the frame in the reconstruction problem. This allows a simplification of the reconstruction problem by identifying a set of optimal features calculated from few temperature sensors, thus reducing the amount of data required for robust reconstruction, allowing for quick processing and low inference time.

3.1. Linear modeling of thermal expansion

Considerations about an isotopic solid and the linear relation of its thermal expansion to mean temperature, introduced in Appendix A.1 of the Appendix, suggest that thermal drift of an axis system can be modeled as a linear time dependent system. Notice that here, heat flow into the system can only be estimated from temperature readings, hence attention has to be payed to the placement of the sensors. Reflecting the linear properties, the time dependent position of a fixed point on a system can be modeled by a linear combination of the time dependent temperature measurements convolved with different impulse responses. I.e.

$$S(t) = \sum_{m=0}^{M} T_m(t) \otimes \Gamma_m(t)$$

where m is the number of the temperature sensor, $T_m(t)$ is the measured temperature time series and $\Gamma_m(t)$ is an impulse response that must be determined from data and theoretical considerations to build the model. In the following, these functions are denoted as thermal drift impulse responses. Notice that the practical goal of predicting the thermal drift is to determine the offset by which the end-effector drifts in a given observed time t_s. This means, that the function to be determined is the difference between the function $S(t)$ and a version of $S(t)$ that is shifted in time by an offset t_s into the future:

$$\Delta S(t) = S(t + t_s) - S(t)$$

In Fourier space, this expression becomes

$$\Delta\hat{S}(\omega) = \sum_{m=0}^{M} \hat{T}_m(\omega)\hat{\Gamma}_m(\omega)\hat{D}(\omega)$$

where $\hat{}$ denotes the Fourier transform, and the function $D(\omega)$ is given by

$$\hat{D}(\omega) = \frac{\exp -it_s\omega}{\sqrt{2\pi}} - \frac{1}{\sqrt{2\pi}}.$$

The function D is a representation of the successive difference $\Delta S(t)$. In Appendix A.4 of the Appendix, this is derived as a convolution with shifted dirac functions. Notice, that D can be calculated explicitly in the frequency domain or easily implemented in the time domain, while T_m is measured directly in the time domain, at least up to the time t

$$E = \begin{bmatrix} \langle T_1(-t)e_1(t-t_1)\rangle & \dots & \langle T_1(-t)e_K(t-t_1)\rangle & \langle T_2(-t)e_1(t-t_1)\rangle & \dots & \langle T_M(-t)e_K(t-t_1)\rangle \\ \vdots & \ddots & \vdots & \vdots & \ddots & \vdots \\ \langle T_1(-t)e_1(t-t_N)\rangle & \dots & \langle T_1(-t)e_K(t-t_N)\rangle & \langle T_2(-t)e_1(t-t_N)\rangle & \dots & \langle T_M(-t)e_K(t-t_N)\rangle \end{bmatrix}$$

Box I.

at which the prediction is executed. The goal of the implementation is to reconstruct a representation of Γ_m, that can be used to calculate ΔS. This can be done by reconstructing Γ_m and applying D afterward in the calculation of ΔS. Alternatively, a set of combined functions $\Gamma_{m,D} = \Gamma_m(t) \otimes D(t)$ can be reconstructed and directly applied to calculate ΔS. These combined functions can be understood as successive differences of the thermal impulse responses. In the following sections, it is discussed how an approximation of these functions can be calculated for a prediction of ΔS (see the unnumbered equation in Box I).

3.2. Reconstruction of successive differences of the thermal drift impulse response

In the previous sections, the functions $\Gamma_{m,D}(t)$ are treated in terms of their Fourier transforms. This representation lends itself to analytical analysis, however, for predictions and reconstructions of future values of $S(t)$, from on discrete experimental data, a discrete representation is required. Clearly, analyses based on bases of linearly independent vectors, like the Fourier series, have the potential to yield a complete representation of these functions. Notice, however, that the number of coefficients in a numerical representation of these functions must be significantly smaller than the number of independent observations of $S(t)$ for the calculation to be numerically stable and ensure generalization to unseen data. In order to reduce complexity and increase robustness of such reconstructions, a common approach is the enforcing of known properties of the actual solution as constraints to the calculated solution. In this context, representing a function or distribution by frames instead of bases of linearly independent (i.e. orthogonal) vectors can allow a direct application of said constraints. A frame is a generalization of a basis of a vector space to sets that may be linearly dependent (Casazza and Kutyniok, 2012). Depending on the choice of the set of functions, this can be used for a complete reconstruction of the original function. However, frames can be a more compact representation and can provide increased numerical robustness (Mallat, 2008). In the following, it is discussed how to reconstruct a representation of this set of functions from measured observations using frame theory. Thereafter, some properties related to the term $D(\omega)$ are discussed with regard to their impact on a practical model. Following the definition of a frame introduced in Section 3.2.1 of the Appendix, the function $\Gamma_{m,D}(t)$ is represented by a frame, such that

$$\Gamma_{m,D}(t) = \sum_{k}^{K} c_{k,m} e_k(t)$$

i.e.

$$\Delta S(t) = \sum_{m=0}^{M} \sum_{k=1}^{K} T_m(t) \otimes c_{k,m} e_k(t)$$

Notice, that for a fixed point in time t_n, the convolution can also be written as an inner product:

$$\Delta S(t_n) = \sum_{m=0}^{M} \sum_{k=1}^{K} c_{k,m} \langle T_m(-t) e_k(t-t_n)\rangle$$

Using more than one observation for ΔS relation can be translated into a set of linear equations:

$$s = Ec$$

where s is a vector of all observations of ΔS, c is a vector containing all weights c_k and each row of the matrix E contains the inner products detailed in E, where N is the number of independent measurements of the thermal drift ΔS. The problem of reconstruction of $\Gamma_{m,D}(t)$ and calculation of ΔS is thereby simplified to solving a set of linear equations to determine the coefficients of c. For a sufficient number of observations, this can be done using a numerical least squares calculation. Notice that the values of c_k are thereby automatically scaled to fit the observed data, so no prior re-scaling of $e_k(t)$ is required. Obviously, the choice of the functions $e_k(t)$ have a meaningful impact on the validity of the model and its performance. This will be discussed in the following section.

3.2.1. Choice of functions in frame

As discussed, the choice of functions in the frame that is being used for the representation of the functions $\Gamma_{m,D}(t)$ can be expected to play a large role for the performance of the prediction of $\Delta S(t)$ by our model. In the Appendices A.4 and A.5 properties of the successive difference term D, are used to show that a windowed linear function with window widths 1.4302 t_s, 2.45902 t_s, 3.47089 t_s or 4,47741 t_s shares at least 3 of the zero crossings of $\widehat{D}(\omega)$, and can therefore be considered to be adequate to impose known boundary conditions on the reconstructed functions $\Gamma_{m,D}(t)$. These can be conveniently determined using the slope of a linear fit in the given window length. Hence, these functions can be used for the definition of the frame. The estimation of slope coefficients is performed through ordinary least squares method (OLS) as follows:

$$\beta_{m,ts} = \frac{\sum_{i=1}^{N}(X_i - \bar{X})(Y_{m,i} - \bar{Y_m})}{\sum_{i=1}^{ts}(X_i - \bar{X})^2}$$

Assuming temperature sensors are sampled at frequency f for a period of time t_s, X is the discretized time vector with discrete time samples going from 1 to $N = ft_s$ and Y_m is the mth temperature sensor measurements vector, $\beta_{m,ts}$ is the slope coefficient of temperature observations collected for t_s, with the mth temperature sensor, and is used as dynamic-range thermal features used for reconstructing the successive differences of the thermal drift impulse response.

3.3. Exogenous and endogenous linear models

In view of the considerations laid out in the previous section, a modeling methodology is proposed for the case study of a single motion system with 3DOF. The error component introduced by motion induced quasi static conditions and temperature oscillations with amplitude ranging between $\pm 1\,^{\circ}\mathrm{C}$, impose clear transient dynamics with variable duration. The time constant of slow and fast components of the drift scales directly with the amplitude of the underlying temperature gradient, driving a continuous position change.

3.3.1. Data processing

Velocity is used as a metric for the thermal drift and it is calculated as the slope of a linear fit of an arbitrary large amount of position measurements. Thus, it is possible to optimize the window size for the thermal drift calculation, to maximize the signal-to-noise ratio, as depicted in Fig. 2. A moving window of 5 min is chosen for the proposed use case, hence imposing $t_s = 300\,\mathrm{s}$. Due to variable thermal drift transient time for different directionalities, each dimension is modeled individually, in a form of a multi-output regression system. For each

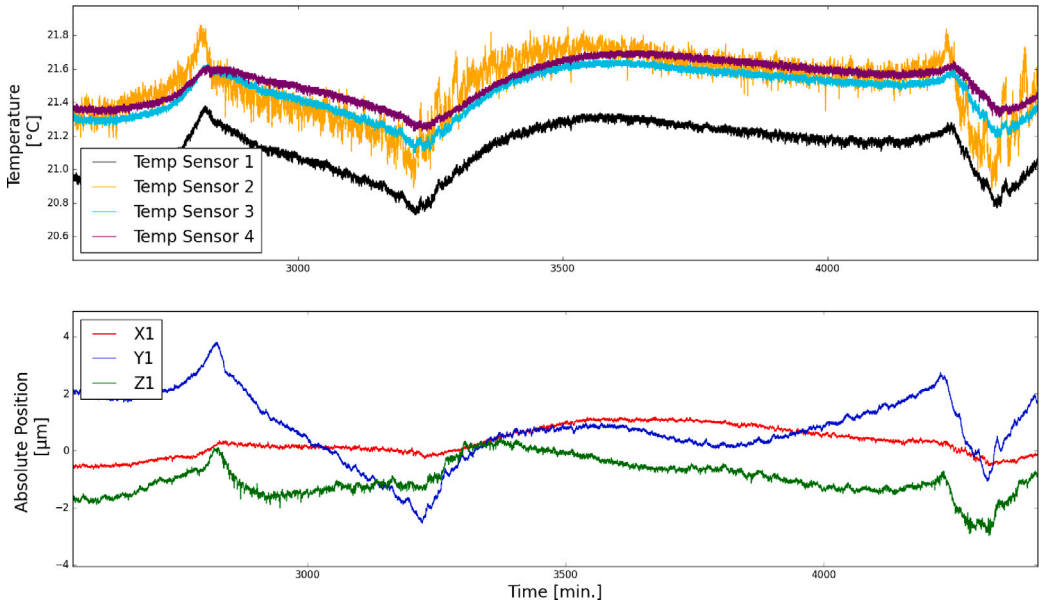

(a) Axes position drift and temperature raw data.

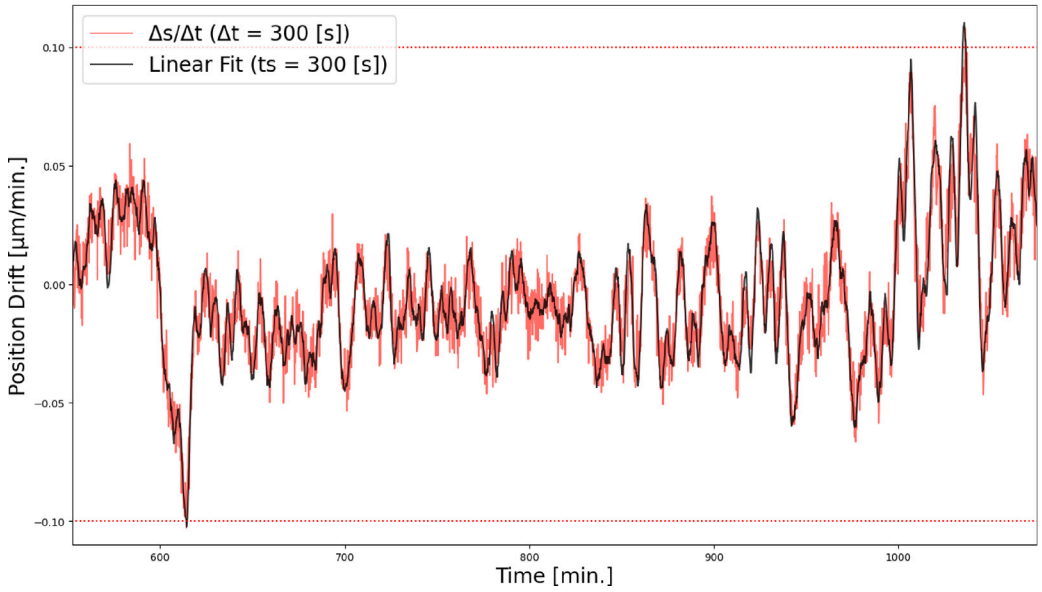

(b) Y1-axis position drift.

Fig. 2. Temperature and position raw measurements and calculated position gradients. In Fig. 2(a) it can be observed that the effect of temperature variations is significantly different along the system dimensions. In Fig. 2(b) the position drift of the Y-axis is calculated as the velocity at which the position change over time. A velocity metric calculated over 5 min intervals is compared with the slope of a linear fit over the same window. It can be observed that a sample to sample velocity metric is more noisy than a linear fit. Samples, which calculated drift is above 100 nm/min in absolute value (dotted red lines), are later discarded.

temperature sensor, dynamic-range thermal features are calculated according to the definition of the frame function given in Section 3.2.1 over time windows which width starts from 1.4302 t_s (details in Appendix of the Appendix) up to 150 s, following a logarithmic decrease. Dynamic-range thermal features show a clear correlation with position gradients along different axes; features with the highest correlation are used to perform a cross-correlation analysis. In Fig. 3 cross-correlation coefficients are reported as a function of the shift between the input and target signal. It can be seen that dynamic-range thermal features extract from different sensors allow to capture longer and shorter components of the drift. Additionally, faster and slower features match the target signal when it is delayed by a factor that scales directly with the respective windows' width. Thus, dynamic-range thermal features can be used to efficiently model components of the drift with different time constants and consequently achieve high prediction accuracy with a low complexity and higher robustness of the underlying model.

3.3.2. Regression estimators

The best features are identified for each axis individually through Sequential Feature Selection (SFS) with a 3-fold cross validation principle. SFS is a greedy procedure where, at each iteration, the best new feature to add to the selected features is chosen based a cross-validation score. The procedure is repeated until the score is not improved by a predefined tolerance value. Identified features are then processed by removing the mean and scaling to unit variance. The final linear regression models' weights are estimated through a Stochastic Gradient

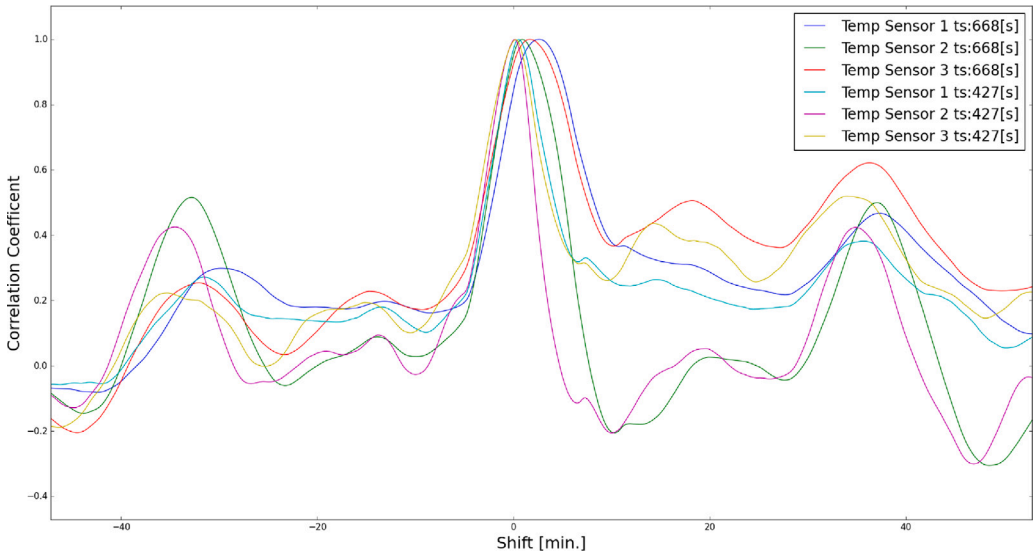

Fig. 3. Correlation coefficients of Y1-axis dynamic-range thermal features vs. its thermal drift. A measure of similarity between the two signals is displayed as a function of their relative delay. It can be observed that the position response to temperature changes is a composition of thermal effects with variable lasting duration taking place ad different locations of the axis system links. The highest correlation is achieved by features calculated from time windows of 427 and 668 s, as well as features produced from sensors 1,2 and 3. Sensors placed at different locations capture temperature changes that contains information on the shorter and longer components of the drift. Sensor 2 captures the shorter drift component, Sensor 1 and 3 capture the longer drift components.

Descend (SGD) optimization process where an L2 regularization term is added to the loss function that shrinks model parameters towards the zero vector. SGD estimation with L2 regularization terms has been chosen among other fitting techniques for its quick convergence properties, its ability to handle large dataset and its intrinsic robustness against local minima or saddle points, potentially leading to better solutions in non-convex optimization. Finally SGD is well-suited for online learning, where the model is trained incrementally as new data is observed, rather than on a static dataset; due to the robustness requirements of industrial use, online retraining can be advantageous to incorporate changes in operational conditions without requiring system downtime.

3.3.3. Ensemble model

Purely endogenous linear models are trained with temperature data in which the variance is reduced to match steady states, hence when the position drift is below 30 nm/min. Position and temperature measurements collected when position gradients are calculated to be above 30 nm/min and below 100 nm/min are used to train an AR and ARX model with linear kernels, that learn quasi-stable and transient states. Position and temperature measurements collected when position gradients are calculated to be above 100 nm/min are discarded. Finally, the estimation of y_t is performed by means of a voting paradigm where both endogenous and exogenous models' predictions are combined as follows:

$$y_t = W^T \hat{Y}$$

where $\hat{Y}$ is a vector of n elements where n is the number of voting estimators, containing single estimators predictions and W is a vector of n elements containing single estimators weights defined as

$$w_i = \left(\frac{RMSE(y_{t-1}, \hat{y}_i)}{\sum_{i=1}^{n} RMSE(y_{t-1}, \hat{y}_i)} \right)^2$$

4. Proof of concept

In the proposed study, the thermal drift behavior is measured by continuously realigning a calibration plate mounted on the motion system with an optical set-up. 4 NTC temperature sensors are used to continuously collect temperature data at different locations of the machine. NTC thermistors have been chosen against PTC thermistors since they normally offer higher precision and accuracy in temperature measurement, especially within a specific temperature range. NTC thermistors exhibit a gradual, linear decrease in resistance at increasing temperatures and have relatively low tolerances, making them suitable for precision applications.

4.1. Test bed: infrastructure and data acquisition

The test bed is endowed with a high-precision linear axis system (X, Y and Z axes). An image of the test bed is shown in Fig. 4(b). The encoders position feedback has a 39 nm resolution for all axes. The temperature of the machine room is maintained within 21.5 ± 1 °C. NTC thermistors with 30 kΩ temperature probes are attached to different positions on the surface of the machine axes links, to collect temperature from bodies of the motion system and the air temperature. A calibration target, composed of reflecting plates separated by an aperture of about 1 μm, is attached to the axes system by means of a carbon fiber injected 3D printed holder. The choice of material for the printed parts is to achieve the lowest drifting contribution to the measurements and improve stiffness. The position displacement between the reflective plate and the vision system is measured using an image processing routine that continuously realigns the calibration target to the vision system. For precise measurements, an optical setup with a microscopic objective is used. Image data with a native pixel pitch of 300 nm is collected and post processed with a vision routine to achieve sub pixel resolution measurements. The vision routine short-term repeatability is measured to be 12 nm. Here, a q-metric, as described in Mandelli et al. (2025), is used for calculating repeatability; in this context it can be interpreted similar to a standard deviation. To ensure that, the calibration plate is always as close as possible to the vision system focal point when images are collected, the Z-axis is realigned before re-centering the axes to the target using an auto-focus routine within a predetermined scan size, with a constant velocity of 2 μm/s. After the planar XY target position is measured, the motion system is re-centered and the current axes positions are sampled from the control system and stored to calculate the thermal drift. In Fig. 4 it is reported a schematic of the data acquisition and model training infrastructure. Temperature and position data are collected for 7 days, yielding on average 8000

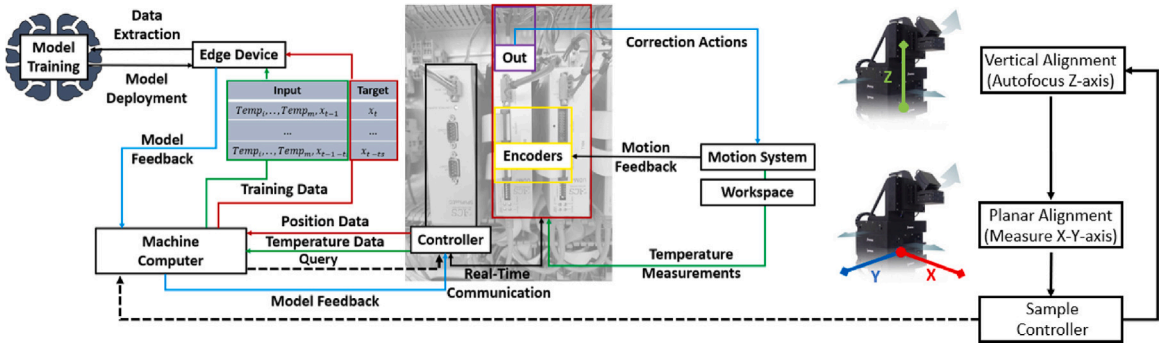

(a) Flow-chart.

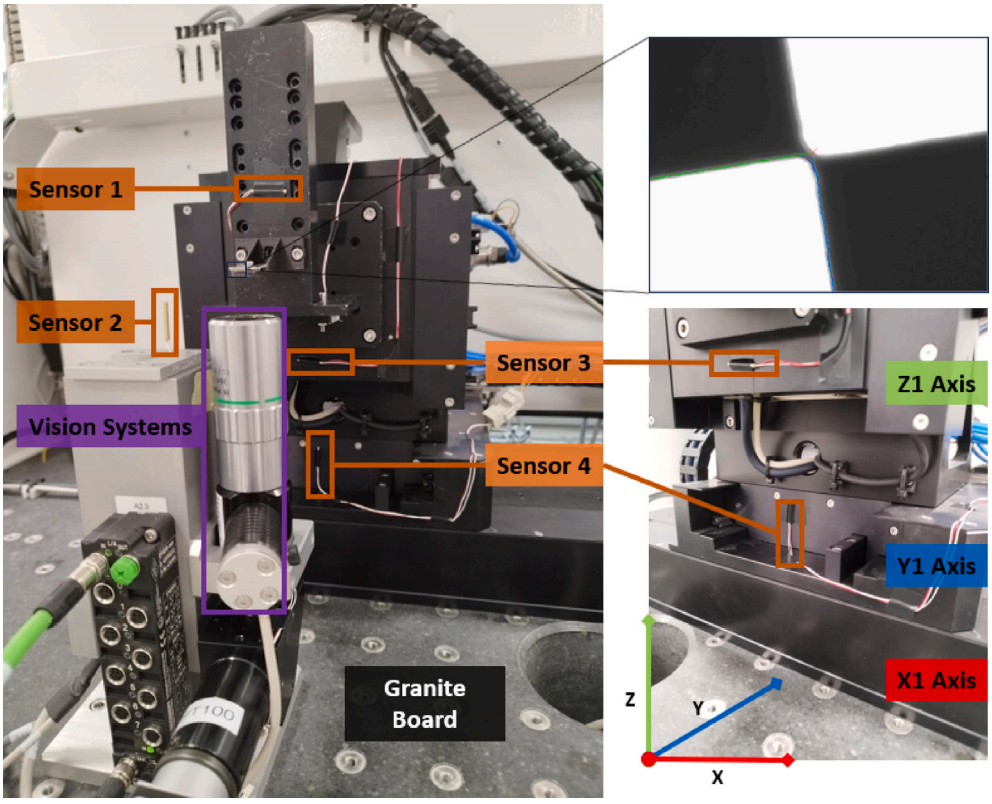

(b) Lab-setup.

Fig. 4. Flow chart of the proposed methology and investigated test bed. In Fig. 4(a) the underlying infrastracture is reported. Direct connection is established between the axes controller-drives (master–slave) system and a dedicated computer (Edge Device) that handles data operations and model the deployment. The control system is composed of a controller (master) and drives (slaves). Each drive (red box) has dedicated connections with encoders (yellow box) which provide real time position feedback from the axes, external sensors, which provide real time information of environmental measurements and with the axes (purple box) to realize control actions calculated by the controller (black box). Position data for n axes (x_t) is queried from the controller through the machine computer each time a re-alignment is completed at a given time t, and streamed to the edge device. Temperature measurements from m sensors ($Temp_i, \ldots, Temp_m$) are directly collected with the machine computer through a dedicated Data Acquisition (DAQ) system and streamed to the edge device. In the edge device, data is fused and organized inside a time series databases. In Fig. 4(b), the investigated test bed is shown with particular attention to sensors placement and position measurements. A reflective plate (calibration-tool) is attached on the Z-axis through a 3D printed holder. Temperature sensors are placed on different locations of the axes; temperature sensor 1 is placed in proximity to the calibration-tool holder, temperature sensor 2 is placed in proximity to the calibration tool plate and the microscopic objective, in open air, temperature sensor 3 is attached to the Z-axis and temperature sensor 4 is attached to the Y-axis. An optical setup with a microscopic objective is used to continuously recenter the calibration-tool.

realignments over the course of 24 h. Temperature sensors are sampled with a period of 50 ms. Half of the data is used for training and validation of the models, the remaining half is used for testing the models. The advantage of using a multi-step prediction pipeline has been chosen as an alternative to structurally more complex models, allows training models on standard CPUs. For the training, an Intel® Core™ i7-10510U CPU @1.8 GHz with max clock at 2.3 GHz has been used, thus permitting a sustainable retraining procedure to be run also within the deployed service. Pipelines containing models require significant lower training time as opposed to pipelines containing non-linear models due to the overall higher amount of trained parameters. Pipelines' execution time for a single sample are calculated from The best performances are measured by employing purely exogenous models, with an execution time of 2.47×10^{-4} s, and pipelines based on endogenous linear models with exogenous inputs, with an execution time of 5.6×10^{-5} s. The worst performance is measured by employing the ensemble model with the

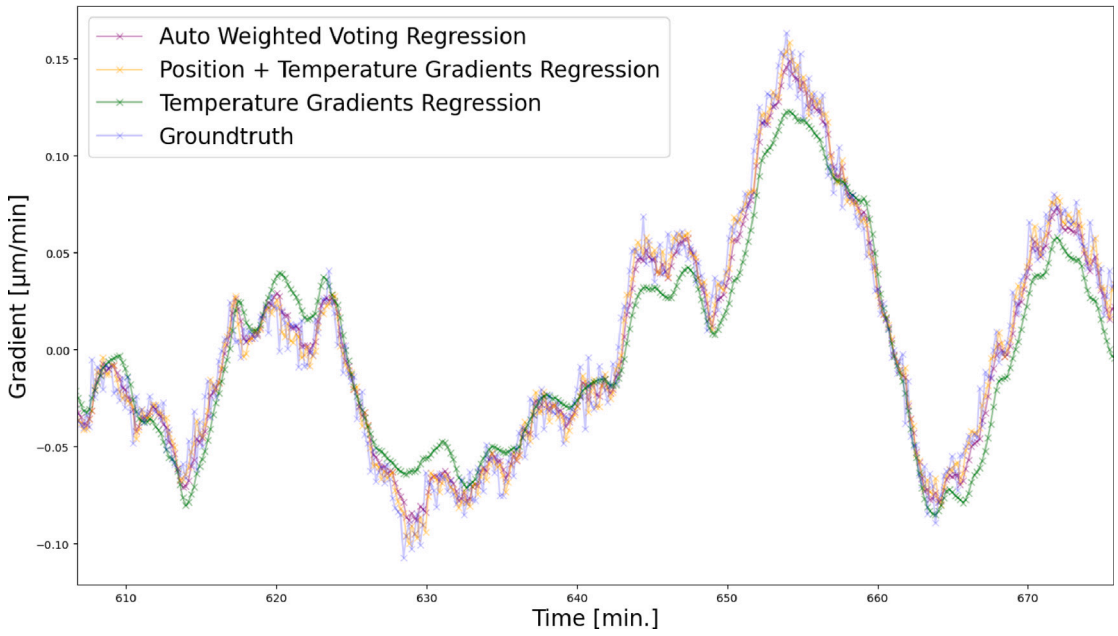

(a) Y-axis drift.

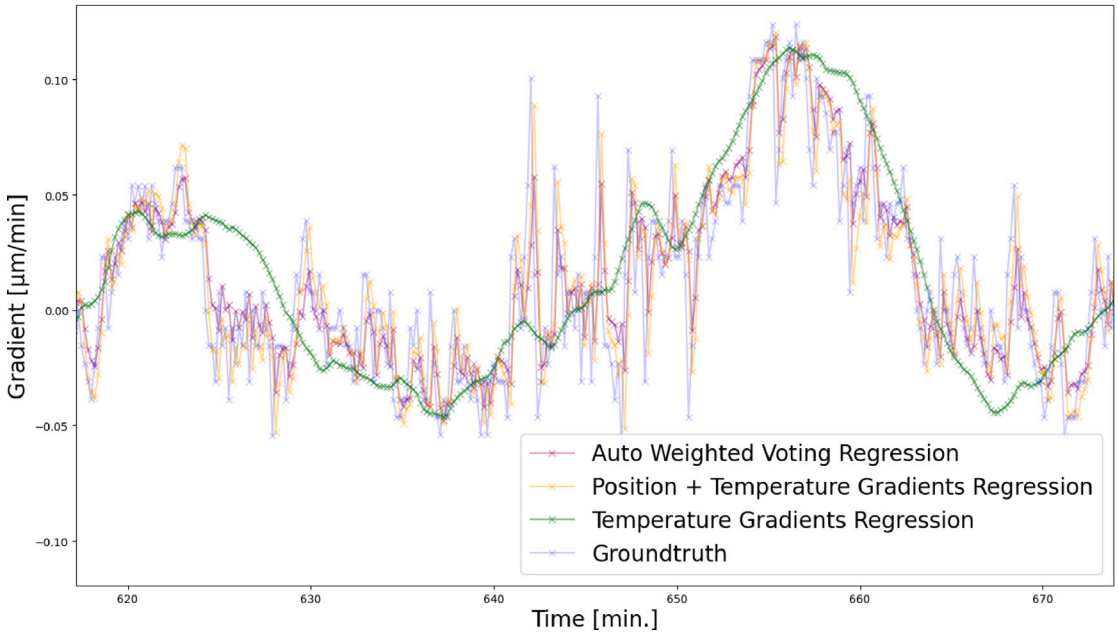

(b) Z-axis drift.

Fig. 5. Y-axis and Z-axis position drift, X-axis position drift is not reported graphically for better visualization purposes. Ground truth against different models predictions. In Fig. 5(a) temperature regression shows good capability of modeling purely thermally induced errors under different stability conditions. In Fig. 5(b) it is possible to observe the effect of position dependent variability. The Z-axis is directly affected by forces related to its weight, as well as stronger coupling with the underlying axes. Those effects drive rapidly changing position errors. Position gradients augmented with dynamic-range thermal features allow to achieve more stable predictions and react to quick changes in position. A purely endogenous model is not displayed in the plot to do not overload the visualization.

voting paradigm based on RMSE metrics, with an execution time of 0.015 s.

4.2. Experimental results

In this section, experimental results of modeling the thermal drift effects measurable at an extremity of a high-precision motion system are reported and discussed. In Fig. 5(a) it is displayed that when static thermal conditions are met, the thermally induced position drift is entirely generalized by temperature gradients representative of a close-set of past thermal states of the system. A simple linear modeling approach allows to precisely learn a generalized relationship between thermal expansion and the temperature changes in the system. The model precision and generalization ability decrease with increasing variability in the data, hence when transient dynamics are introduced. Non-linear, position dependent modes of the drift are nonstationary processes that can appear unpredictably as a result of high temperature gradients being imposed on the system as well as sudden pose change related frictional heat. Transient states are therefore difficult to model

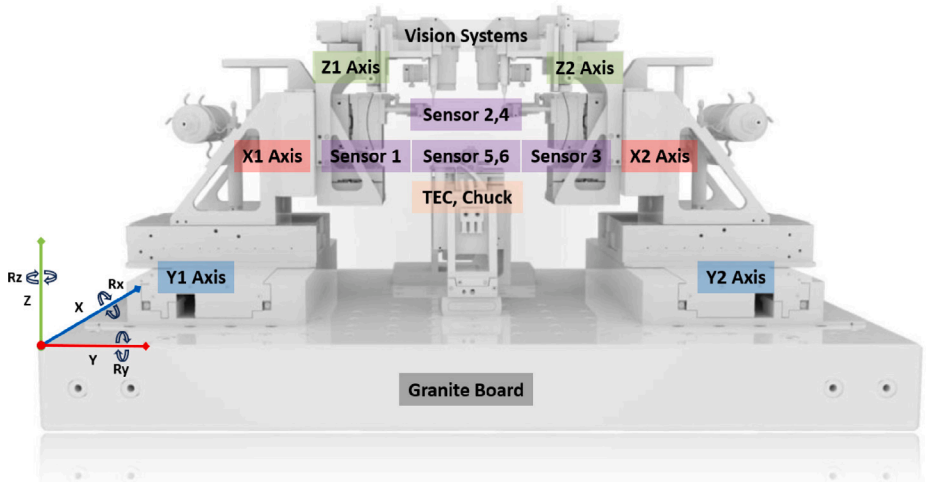

Fig. 6. Automatic die tester system with two 6DOF motion systems for high-precision positioning. Two motion systems are used for the automatic alignment of the metrology instrumentation with singulated dies. Motion stages are placed on a granite board installed on a dampening system that guarantees low resonance frequency and lowers the mechanical coupling between axes. The housing is placed on ground isolation feet, to reduce the effect of external ground vibrations. A chuck is built between the two motion systems where a TEC is employed to integrate a PID temperature control that allows to stabilize the temperature to desired test conditions. The temperature control is realized through a peltier cell positioned at the chuck base while the PIC is held in position through a vacuum port. High-precision temperature measurements are collected by 6 NTC temperature sensors placed at different positions of the system bodies to observe the workspace air temperature, chuck temperatures and fiber holder temperature. Those sensors are expected to collect signals with high variance. Two more sensors are attached inside the motion stages. Those are expected to collect lower variance readings, mostly having an impact on the steady state of the system.

Table 2
Comparison of RMSE [nm/min.] and R^2 values for different models.

Model	RMSE [nm/min]			R^2		
	X	Y	Z	X	Y	Z
Ground truth	11.18	22.99	20.87	–	–	–
Temperature gradient regression	8.13	11.64	17.89	0.4702	0.7436	0.2654
Position gradients regression	6.81	9.41	13.72	0.6289	0.8323	0.5678
Position + Temperature gradients regression	6.55	8.81	13.67	0.6560	0.8530	0.5711
Auto-Weighted voting	6.31	8.69	13.17	0.6811	0.8571	0.6019

with a purely linear regression of dynamic-range thermal features. In Figs. 5(a) and 5(b) it is shown that modeling positional features in an auto-regressive fashion, allows learning the transient behavior with a degree of generalization that a simple thermal model cannot achieve. Nonetheless, modeling the positional drift from observation of past states only, can results in unstable predictions; the precision and stability of this class of models depends strongly on the observability of the system, hence being subject to noise and inaccuracies introduced by the measurement system. Position features are therefore augmented with thermal features thus resulting in a model that generalizes well quasi static states. Finally, separating the modeling problem by means of the introduced voting paradigm allows to automatically tackle static, quasi static and transient states of the drift. A combination of positional dependent transient modes and static the thermal dependent settled behavior can be further generalized through dynamic-range exogenous and endogenous features modeled with an auto-weighted voting paradigm, thus resulting in the overall best prediction ability as reported in Table 2. In Fig. 5 it is possible to observe prediction properties of a purely exogenous linear model, a model of endogenous features augmented with dynamic-range thermal features, as well as the effect of the proposed auto-weighted voting ensemble schema.

5. Model validation: Testing PICs in unstable thermal conditions

Testing of component functionalities is a recurrent and complex problem in the manufacturing chain of PICs; the lack of reproducible motion routines that allow for stable and tolerant alignment between the metrology instrumentation and the PIC, as well as the necessity of testing at different temperature ranges, make testing a time consuming operation that poses scalability challenges. Constraints on alignment repeatability and standstill stability under variable thermal conditions prevent industrial processes to reach the same cost breakdown as EICs: today, the major part (up to 80%) of a photonic module cost still lies in packaging and test operations, not in the circuit itself (Bernabé et al., 2023). PICs with complex functionalities demand more complex circuits and conversely, the complexity of the circuits directly impacts the performance specification of the PICs. The number of photonic components integrated into the same circuit is approaching one million, but so far, this has been without the large-scale integration of active components: lasers, amplifiers, and high-speed modulators (Wang et al., 2024). Adding more components to the PIC is still possible, at the cost of larger chip areas and higher risks of yield loss. Alternatively, increasing the integration density per unit chip area by reducing the optical components features size can be done, however this requires major investments into the development of these components. The major limiting factor in latest PICs, such as InP, is the low optical confinement in the ridge waveguide structures on the substrate (Jiao et al., 2020). This leads to using waveguide with model field diameter (MFD) in the range of 2 µm and lower, directly imposing very high motion precision and stability requirements for alignment processes needed to perform PICs testing measurements. Under testing conditions, the optical loss of the measured signal must be reproducible within a predefined interval, over the course of the measurements. In case of a measured beam diameter of 2 µm (with a $1/e^2$ power drop off) and a maximum optical loss of 0.2 dB, the maximum tolerated position deviation along all axes can be calculated to be 75 nm using the calculations detailed in the Appendix A.7. Such degree of stability requires considering not only the intrinsic manipulator error sources, i.e. axes coupling and resonance,

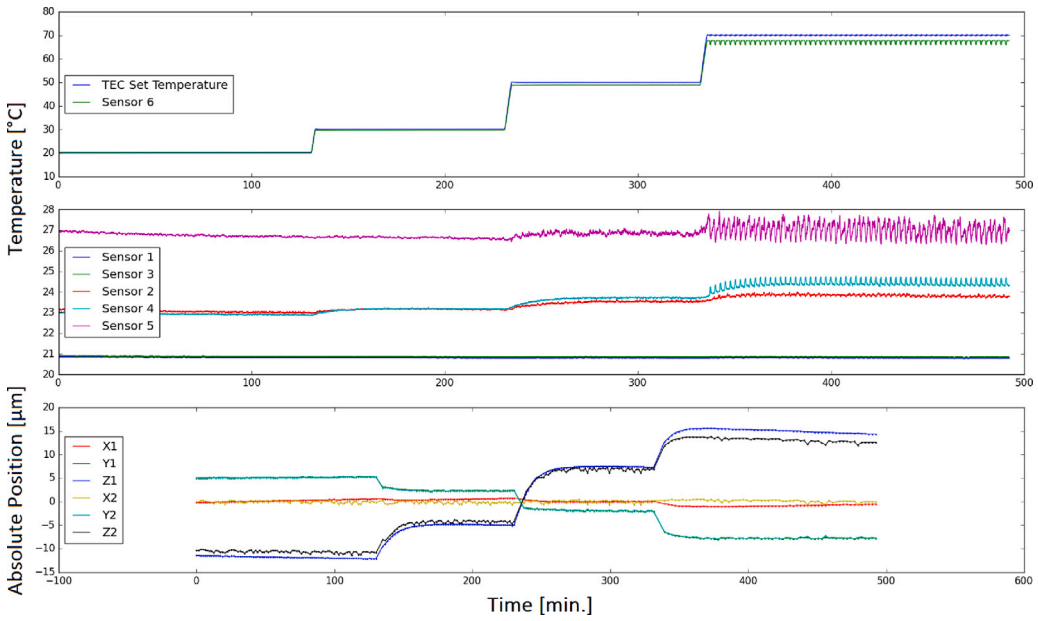

Fig. 7. Temperature measurements and position measurements over time. Temperature sensors used to calculate the input features for the regression problem are: Sensor 1 logs the temperature at the fiber aligner 1 axis plate, Sensor 2 - temperature at the fiber aligner 1 holder, Sensor 3 - temperature at the fiber aligner 2 axis plate, Sensor 4 - temperature at the fiber aligner 2 holder, Sensor 5 - machine room temperature, Sensor 6 - realized chuck temperature. Axis plate sensors are positioned between the X, Y and Z-stages, while holder sensors are positioned in proximity of the fiber holders used to grab the optical fibers.

but also environmental disturbances, i.e. external vibrations (Beijen et al., 2018) and thermal effects. While mechanical inefficiencies can be improved by axis tuning and dampening, thermal effects require implementing specific design changes. In the following section, the methodology proposed in Section 3 is validated with data gathered with an industrial die testing machine operating under unstable thermal conditions cause by heating of a chuck hosting the PIC.

5.1. Multi DOF axes system position error contribution to the optical power loss

Due to the high constraint on stability, at both the motion stage and the chuck holding the PIC, injecting high temperature gradients in the testing environment impose pausing machine operations for long settling time before achieving stability conditions required to perform characterization measurements. A schematic of the tesing system considered in this study, is reported in shown 6; a two-sided fiber to PIC alignment is followed by 5 min measurement period during which measurements for PIC characterization are performed while motion stages hold their position. For the proposed use case, the requirements for optical stability dictate a maximum optical loss of 0.2 dB over the measurement period, imposing a maximum position deviation tolerance of 20 nm/min along all axes. The full PIC characterization is achieved by remeasuring the signal properties at different operational temperatures, ranging from 20°C to 120°C as shown in Fig. 7. In Appendices A.6 and A.7 of the Appendix, a formulation for the case of multiple DOF linear axis is presented to quantify the requirements of motion stages employed in the filed to meet signal stability below 0.2 dB maximum loss under variable thermal conditions, thus to justify the need of a thermal drift compensation approach. The identified conversion coefficients allow to map 6 linear DOF position errors into the expected optical signal loss, so to directly evaluate the thermal drift effects on the optical signal loss specification.

5.2. Auto-weighted voting model training

Training and testing sets are collected under different working conditions. Fig. 7 shows the training set raw data. Measurements are performed at different temperatures, ranging from 20 °C to 70 °C. In Fig. 8(a), it is shown the testing set position drift data for the Z1-axis. Measurements are performed at different temperatures, ranging from 20 °C to 120 °C and include also a decreasing temperature phase from 120 °C to 70 °C. Endogenous models are trained with data that includes thermal drift with maximum absolute value of 850 nm/min; the purpose of endogenous models with and without dynamic-range thermal features, is modeling high amplitude transient states. Differently, exogenous models are trained with data that includes thermal drift with maximum absolute value of 150 nm/min, targeting quasi stable and stable states. Models are evaluated with data produced when different stability conditions are observed. For the specific use case, any PIC measurement performed at 250 nm/min is considered unreliable, due to the high instability conditions, hence under those circumstances, machine operation is interrupted until thermal conditions have sufficiently stabilized. Data points characterized by thermal drift above 250 nm/min are therefore removed from the testing set before performing stability analysis, as shown in Fig. 8(b). Model performances are reported in Table 3, where it can be confirmed that a purely endogenous model increases its prediction accuracy when exogenous temperature data is used to augment the model input. Finally, when a temperature regression model is combined with AR model and an ARX as separate estimators through an auto-weighted voting ensemble model, the highest prediction accuracy is achieved. The voting models are specialized in predicting high and low variance drift dynamics, and dynamically adjust the contributions of different estimators, based on their recent prediction accuracy. The entire testing set, shown in Fig. 8(a), is used to evaluate the effects of a model-based compensation, on the system transient time. The auto-weighted voting regression performances on high and low variance data, are compared in Table 4.

5.3. Optical loss stability improvement: evolution of thermal drift compensation

The system settling time to reach sufficient thermal stability after high temperature changes are introduced, is measured to be 30 min to 80 min depending on the target temperature of the heated chuck hosting the PIC. The worst case scenario is observed when the temperature

Table 3
Comparison of RMSE [nm] values of different models when low variance data is included in the test set (thermal drift below 250 nm/min).

Model	RMSE [nm/min]					
	X1	Y1	Z1	X2	Y2	Z2
Ground truth	11.54	12.29	53.34	14.38	13.53	47.55
Temperature gradient regression	10.75	12.26	20.07	14.54	13.30	22.22
Position gradient regression	9.83	14.08	15.12	14.48	15.21	15.59
Position + Temperature gradient regression	9.03	12.87	13.33	13.94	15.16	13.72
Auto-Weighted voting	8.45	12.39	10.25	12.74	13.15	12.96

is reduced from 120 °C to 70 °C, imposing a settle time of 82 min. Coefficients identified in A.7 are used to calculate the contribution of each axis to the optical loss, and evaluate the system stability based on the signal loss specifications. In Figs. 8(a) and 8(b), stable and unstable states of the system are reported and matched with the drifting states of the Z1-axis, which has the largest contribution along with the Z2-axis; In Fig. 8(a) it can be observed that by applying the model correction, the waiting time to reach stability can be reduced from 82 min to 32 min in the worst observed case. Testing under high temperature conditions (above 50 °C) results in overall highly unstable states, as it is displayed in Fig. 8(a). It is found the higher temperatures have an impact on the measurements of the drift as can be seen in the relative instability of measurements collected at temperatures above 50 °C in Fig. 8(a). The benefits of a model based compensation when testing under high temperature is therefore limited to reducing the settle time rather than improving the optical loss stability during test. Differently, when temperatures below 70 °C are observed, the optical stability of the system can be improved beyond limits imposed by the environment. Using the conversion coefficients derived in Appendix A.7 of the Appendix and residual errors reported in Fig. 8(b), the effects of position corrections can be evaluated. Maximum loss values in dB are considered. The optical loss is calculated from samples collected 30 min after a temperature change takes place; this is in line with the waiting time required in the worst case scenario. When the temperature is initially stable at 20 °C, the optical loss can be improved from a maximum of 0.069 to 0.043 dB. When the temperature is increased from 20 °C to 30 °C the optical loss can be improved from a maximum of 0.76 to 0.051 dB. When the temperature is increased from 30 °C to 50 °C the optical loss can be improved from a maximum of 2.13 to 0.12 dB.

6. Discussion

Combining predictions of different models with the proposed auto-weighted voting approach increases the final prediction accuracy and provides intrinsic robustness to changing working conditions. AR and ARIMA models trained on historical position data, provide intrinsic robustness towards temperature sensors faults. Similarly, dynamic-range thermal features introduce a degree of redundancy useful to partially compensate for eventual loss of observability; ensemble voters can be trained with thermal features extracted from a sub-set of all available temperature sensors, thus being naturally robust towards observability loss of thermal data. Additionally, the linear nature of the underlying voting models and their weights estimation process (SGD), suits well online learning and enables agile model recalculation and retraining. The window length for calculating thermal drift and the resulting dynamic-range thermal features, can be automatically adjusted, thus increasing the ability of the ensemble model to adapt towards different scenarios of use. The inference process for linear models can be realized directly on board of the controller without requiring an additional computer. Temperature sensors can be connected to the control system and temperature gradients can be calculated iteratively. Clearly, limitations of removing a dedicated data acquisition system are the inability to store data and retrain models as well as the computational limitations.

6.1. Core principle and practical use cases

The proposed solution is applicable in industrial production scenarios where high-precision needs to be accomplished under different thermal stability conditions. The best capabilities are achieved by using both positional and temperature information. Depending on which control problem is tackled, variably long time windows can be defined for the position gradient calculation to match the control action optimal frequency. This is true for a broad range of applications, going from semiconductor to integrated optical components manufacturing and testing. It is infact common to deal with reproducibly variable thermal conditions, as in epoxy curing, die bonding and soldering, as well as optical components characterization under variable thermal conditions; especially in the context of PICs manufacturing and testing, it is usual to face conditions where components functionalities (either singulated dies or wafers) must be tested under a range of different temperature conditions. In case of optical tests, metrology instrumentations for components characterization are continuously realigned to the dies over multiple waveguides, giving a direct access to a measure of the system to PIC relative position drift. The choice of the window length for position gradients depends intrinsically on the position measurements rate and dictate the update time of the correction actions; by having access to a frequent remeasurement, it is possible to frequently update the correction vector. As soon as the model predicts certain, predetermined stability conditions, correction actions are interrupted.

6.2. Model integration in real-time applications: scalability and integrability

The original definition of a model based compensation schema refers to Fig. 4, where a dedicated computer (Edge Device) is used for data related handling operations as well as for the model deployment and inference. A permanent reliable connection between the machine computer and the Edge Device can be established, providing to the overall implementation computational capabilities that would allow to automatically calculate and update complex models. The linear nature of the voting estimators, would permit to directly implement the inference structure on board of the controller. Clearly the latter choice dictates reducing the model complexity to fit the controller computational capabilities. Temperature sensors can be configured to stream analog signals directly to the slaves controller units; together with feedback signals from motion encoders it is possible to directly elaborate dynamic-range thermal features and position gradients on board of the slave controller units allowing to embed the inference process within the master–slave controller structure.

6.3. Limitations and future development

The limitation of a linear exogenous regression is related to modeling nonstationary and position dependent drift components; the latter occur unpredictably when motion is executed and evolve with highly dynamical transient effects. Endogenous models of the position drift allow generalizing the system behavior during transient states with precisions that a simple temperature regression model cannot achieve. The combination of position features and dynamic-range temperature features, yields the best generalization of high position drift, while a temperature linear model yields more stable predictions when slower expansion takes place at steady states. Best modeling capabilities are achieved when all data sources are accessible and can be combined in an auto-weighted voting ensemble model. Practical limitations are therefore identified in endogenous and exogenous models requirements. Endogenous models require accessing a continuous remeasuring of the position drift and are limited by the measurement precision and frequency. Exogenous models are limited by the sensor functioning and placement. Additionally, slow and fast components of the signal must be extracted to achieve precise and stable predictions, requiring high resolution temperature measurements and long sampling time.

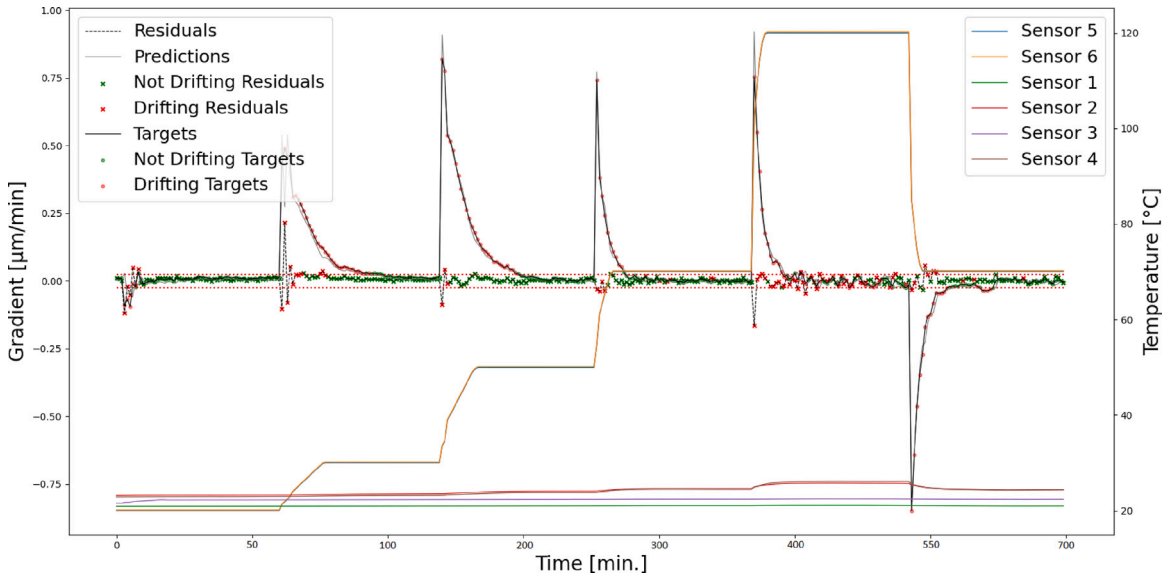

(a) High variance thermal drift (850 nm/min).

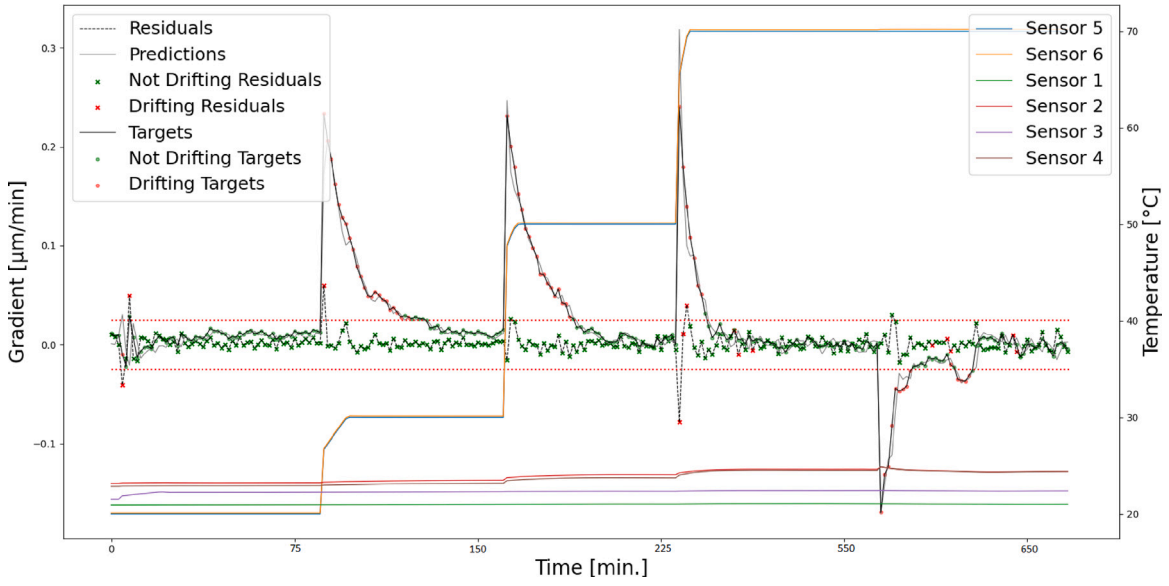

(b) Low variance thermal drift (250 nm/min).

Fig. 8. Stability related to thermally induced position drift of the Z1-axis when temperature gradients below 850 nm/min (high variance data) and below 250 nm/min (low variance data) are observed, with and without a model-based correction. The solid black line represents measured position gradients while the dotted line represents the residual drift after having applied a correction. Green squares and crosses highlight drifting states of the system where the optical loss is below 0.2 dB, respectively with and without correction. As opposed, red squares and crosses mark samples where the optical loss is above 0.2 dB. The red dotted line highlights the maximum tolerated position drift along Z1-axis that is required to keep the optical signal loss below 0.2 dB, being 20 nm/min. Note that even in case the Z1-axis is stable within this boundary, other axes might not be sufficiently stable and therefore produce an unstable state.

Table 4
Comparison of RMSE [nm] values of auto-weighted voting models when high variance data is included in the test set (thermal drift below 850 nm/min).

Test set	Model	RMSE [nm/min]					
		X1	Y1	Z1	X2	Y2	Z2
Low variance	Ground truth	11.54	12.29	53.34	14.38	13.53	47.55
	Auto-Weighted voting	8.45	12.39	10.25	12.74	13.15	12.96
High variance	Ground truth	58.99	50.19	153.42	20.91	56.30	140.96
	Auto-Weighted voting	48.65	46.75	20.67	22.84	52.49	27.52

Future development should concentrate in investigating integration and scalability capabilities when poor observability of the system limits the model functioning. State estimation techniques, such as Kalman-Filters, can be valid solutions to noisy sensing and measurements as well as scarse observability. Similarly, Long Short-Term Memory (LSTM) Encoding-Decoding layers can be embedded into the feature extraction module, in order improve the model capabilities when partial loss of observability is experienced and further increase robustness under non ideal working conditions.

7. Conclusions

Known properties of the heat equation and the heat flow within a still body suggest that, under static working conditions, the heat transfer into the body, the transfer between bodies and the thermal expansion are linear, leading to hypothesizing that the most accurate prediction of the thermal drift is based on a linear combination of impulse responses of a finite set of measured temperatures. For this reason, it is considered to be likely that the time dependent position of a fixed point on a system under stable conditions, can be modeled by a linear combination of the time dependent temperature measurements convolved with different thermal impulse responses. A formulation based on numerical reconstruction of successive differences of the thermal impulse responses is presented and used to identify a suitable frame function choice for the reconstruction problem. Known boundary conditions on the reconstructed impulse responses are imposed by choosing windowed linear functions with fixed widths that share 3 of the zero crossings of the successive difference term. These can be conveniently determined using the slope of a linear fit in the given window length. This formulation allows including in the modeling problem slower and faster components of the temperature signals by extracting multiple features from a single sensor (dynamic-range thermal features), thus reducing the amount of sensors required for an accurate reconstruction and providing robustness towards variable field conditions and hardware faults. It is shown that by separating positional and thermal dependencies of the drift, as well as by separating the static and dynamic component of the drift by employing different model types and data sources, the modeling precision can be significantly impacted. Moreover, by employing an auto-weighted voting criterion it is provided intrinsic robustness towards variable field conditions and adaptive capabilities. The model is validated with experimental data, and it is demonstrated that the proposal ensemble regressor can be used to significantly improve a system stability beyond the limits imposed by field conditions. The validation case of PICs testing is considered where the benefit of employing a model-based compensation is quantified to be: (i) a reduction of the thermal drift along the most critical axis, by 90%, when highly unstable thermal effects take place (up to 850 nm/min) and by 80%, when the modeling is reduced to instability (below 250 nm/min), (ii) a reduction of the worst case system settling time by 60% under test conditions where transient effects (below 250 nm/min) are observed at high instability states when tested temperature are above 50 °C. Finally, when temperature below 70 °C are tested it is proven that the proposed approach can be used to improve the optical loss stability beyond limitations imposed by the test environment.

CRediT authorship contribution statement

Lorenzo Mandelli: Writing – original draft, Visualization, Validation, Methodology, Investigation, Data curation, Conceptualization. **Colin Dankwart:** Writing – review & editing, Supervision, Project administration. **Christian Napoli:** Supervision, Project administration, Funding acquisition.

Ethical statements

The proposed work does not disclose any potential conflict of interest, and the research does not involve human participants or animals.

Declaration of competing interest

The authors declare that they have no known competing financial interests or personal relationships that could have appeared to influence the work reported in this paper.

Appendix

A.1. Heat kernel

One of the basic properties of the heat equation is its linearity, which means that one of the solutions to it is the heat kernel. The heat kernel is convolved with a temperature distribution to calculate future distributions (Berline et al., 2003; Vassilevich, 2003):

$$T\phi(x,t) = \int_{\Omega} K(x,y,t)\phi(y)dy$$

with

$$K(x,y,t) = \sum_{n=0}^{\infty} \exp\left(-\lambda_n t \phi_n(x)\phi_n(y)\right)$$

The values λ_n and functions ϕ denote eigenvalues and eigenfunctions of a Dirichlet problem. The heat kernel for a d-dimensional Euclidean space R^d has a much easier explicit form (Berline et al., 2003; Vassilevich, 2003):

$$K(x,y,t) = \frac{1}{(4\pi t)^{\frac{d}{2}}} \exp\left(\frac{-\|x-y\|^2}{4t}\right)$$

This means that the future heat distribution can be calculated using a convolution with a d-dimensional Gauss function. Note the following:

- The thermal expansion can be simplified as being linearly dependent on temperature change, with a linear expansion coefficient that depends on material and length of the object. For a 1-dimensional problem and 3-dimensional isotropic solids, this means that the elongation would be proportional to the mean value of the temperature difference (Pluta and Hryniewicz, 2012; Drebushchak, 2020).
- The heat kernel does not change its integral with time. This can be derived from the above expression and is in line with energy conservation. This means that the mean temperature within the body is only dependent on the heat flow into and out of the body, the distribution within the body does not have to be known explicitly.

Combining these observations, it can be stated that for an isotropic solid, the mean thermal expansion across each dimension can be modeled by a linear relation either from total heat flow into the solid or from its mean temperature. For bodies composed of multiple solids, the heat transfer between bodies obviously becomes important. However, due to the linear nature of the heat equation, even this case can be approximated by a linear dependent time system.

A.2. Frame representation of functions

The representation of a function $f(x)$ by a frame is very similar to that by an orthogonal base:

$$f(x) = \sum_k c_k e_k(x)$$

where

$$c_k = \langle f(x) e_k(x) \rangle$$

In order for the mapping to work, the functions $e_k(x)$ must be scaled in a certain way to fulfill a boundary condition called the frame condition, firstly introduced in Duffin and Schaeffer (1952). Notice that this could also be achieved by multiplying every coefficient c_k with a factor depending only on k after calculating the inner product.

A.3. Thermal drift and impulse response functions

The time dependent temperature measurements convolved with different impulse responses convolution can be written as:

$$S(t) = \sum_{m=0}^{M} \int_{-\infty}^{\infty} T_m(t-\tau)\Gamma_m(\tau)d\tau.$$

A term $\Delta S(t)$ being, the difference between $S(t)$ and a version of $S(t)$ that is shifted in time by an offset t_s, can be expressed in terms of a convolution with a pair of shifted Dirac functions:

$$\Delta S(t) = S(t) \otimes [\delta(t+t_s) - \delta(t)]$$

Combining this with the earlier expression for $S(t)$ yields

$$\Delta S(t) = \sum_{m=0}^{M} [\Gamma_m(t) \otimes \Gamma_m(t)] \otimes [\delta(t+t_s) - \delta(t)]$$

A.4. Properties of successive differences

The calculation of successive differences is represented by the term $D(t)$ and its Fourier transform $\widehat{D}(\omega)$. This function can be separated into a phase term and a sine function:

$$D(\omega) = [\frac{\exp(-it_s\omega)}{\sqrt{2\pi}} - \frac{1}{\sqrt{2\pi}}][\ \exp(it_s\omega/2)\ \exp(-it_s\omega/2)]$$

$$= [\frac{\exp(-it_s\omega/2)}{\sqrt{2\pi}} - \frac{\exp(it_s\omega/2)}{\sqrt{2\pi}}]\ \exp(-it_s\omega/2)$$

$$= [\frac{-2\sin(t_s\omega/2)}{i\sqrt{2\pi}}]\ \exp(-it_s\omega/2)$$

$$= i\sqrt{2/\pi} - 2\sin(t_s\omega/2)\ \exp(-it_s\omega/2)$$

$$\widehat{D}(\omega) = i\sqrt{\frac{2}{\pi}}\sin\left(\frac{t_s\omega}{2}\right)\exp\left(-\frac{it_s\omega}{2}\right)$$

Notice that due to the sine term, in $\widehat{D}(\omega)$ determining its absolute value, $\widehat{D}(\omega)$ has the following properties:

1. at the zero frequency and all frequencies $\omega = 2n\pi/t_s$ of $\widehat{D}(\omega)$ has amplitude 0 for $n \in Z$,
2. For frequencies $\omega \ll \frac{\pi}{t_s}$, the absolute value of $\widehat{D}(\omega)$ approximates $\frac{t_s\omega}{\sqrt{2\pi}}$
3. the maximum absolute value of $\widehat{D}(\omega)$ occurs at frequencies $\omega = \frac{\pi}{t_s} + \frac{2n\pi}{t_s}$ for $n \in Z$.

The first two properties mean that low frequency components are suppressed in any direct evaluation of ΔS and thus are difficult to recover. They also mean, that the functions $e_k(t)$ being used to represent $\Gamma_{m,D}(t)$ should have a mean value (zero frequency) of 0. Property 3 may have implications for applications with different choices for the time constant t_s, since it shows that a good choice of t_s might allow for easier reconstruction of $\Gamma_{m,D}$.

A.5. Windowed linear terms

A windowed linear term can be understood as a product of a linear term and a rect function with positive width T:

$$g(t) = t\ \mathrm{rect}(\frac{t}{T})$$

In Fourier space, this is equivalent to the derivative of a sinc function:

$$\widehat{g}(\omega) = i|T|\frac{d\ \dot{\mathrm{sinc}}(\frac{\omega T}{2\pi})}{d\omega}$$

where

$$\dot{\mathrm{sinc}}(x) = \frac{\sin \pi x}{\pi x}$$

i.e.

$$\widehat{g}(\omega) = 2i|T|\frac{d}{d\omega}\frac{\sin \omega T/2}{\omega T}$$

$$= i|T|\frac{1}{\omega^2 T^2}[\omega^2 T^2\cos(\omega T/2) - 2T\sin(\omega T/2)]$$

$$= 2i\frac{1}{\omega}[T\cos(\omega T/2) - 2\frac{\sin(\omega T/2)}{\omega}]$$

$$= 2i\frac{1}{\omega}[T\cos(\omega T/2) - T\frac{\sin(\omega T/2)}{\omega T/2}]$$

$$= 2i\frac{T}{\omega}[\cos(\omega T/2) - \ \mathrm{sinc}(\omega T/2)]$$

where,

$$\mathrm{sinc}(x) = \frac{\sin x}{x}$$

Due to the fact that sinc(0) = 1, this function has a value of 0 at the zero-frequency. Furthermore, it has zero-crossings at values $\omega_0 = \pm 4.4934\frac{2}{T}$. In order for the first zero-crossing to coincide with the first zero-crossing of $D(\omega)$, the following condition must be fulfilled:

$$4.4934\frac{2}{T} = \frac{2\pi}{t_s}$$

i.e.

$$T = 4.4934\frac{t_s}{\pi} = 1.4302t_s$$

Equivalently, for the higher zero crossings of $\widehat{g}(\omega)$ to match the first ones of $\widehat{D}(\omega)$, the above factor can be replaced by 2.45902, 3.47089 or 4,47741.

A.6. Single DOF contribution to optical power loss

In the following, it is derived expressions for the estimation of optical loss, given in decibels (dB), dependent on beam parameters and observed position errors along different dimensions. Here, the beam profile is modeled as a Gaussian function:

$$P = C\exp -2\frac{(x-x_0)^2}{\sigma^2}$$

The σ value represents the distance after which the power drops by a factor of $\frac{1}{e^2}$ of its maximum value when moving along x. This can be calculated using optical simulations or measured experimentally. Notice that this value is related, but not equal to the mode field radius, due to the additional widening of the beam profile due to the effect of finite width of the fiber core. To calculate the power with a relative loss factor f, the positional distance can be replaced by a position error $\hat{x}$:

$$Pf = C\exp -2\frac{\hat{x}^2}{\sigma^2}$$

Solving for the loss factor, we obtain, we get

$$f = \exp -2\frac{\hat{x}^2}{\sigma^2}$$

A.7. 3DOF contribution to optical power loss

Now the losses along multiple axes must me multiplied in order to calculate total loss. However, converting the calculation to logarithmic space for conversion to dB, converts the product to a sum:

$$Loss_{dB} = \log_{10}(e)\sum_{n=1}^{N}\frac{-2}{\sigma_n^2}\Delta x_n^2 = -8.6859\sum_{n=1}^{N}\frac{\Delta x_n^2}{\sigma_n^2}$$

where the Δx_n values represent the positioning errors along a certain dimension, this can be x, y or z. Considering the stability specification of the system at hand, being maximum tolerated loss over a period of

5 min below 0.2 dB, temporal gradients ($\Delta\dot{x}_n$) calculated over 5 min have to adhere to the following condition:

$$-8.6859 \sum_{n=1}^{N} \frac{\left(\Delta\dot{x}_n \cdot 5\,\text{min}\right)^2}{\sigma_n^2} < 0.2$$

Converting to an easier form yields

$$\sum_{n=1}^{N} a_n \left(\Delta\dot{x}_n\right)^2 < 0.2$$

For $\Delta\dot{x}_n$ given in μm/min, the coefficients for conversion of position errors in the expected optical loss are as follows:

$$\begin{aligned}
x_1 &: \quad X1; && a_1 = -2.09059\ \text{min}^2/\mu\text{m}^2 \\
x_2 &: \quad Y1; && a_2 = -59.4658\ \text{min}^2/\mu\text{m}^2 \\
x_3 &: \quad Z1; && a_3 = -133.798\ \text{min}^2/\mu\text{m}^2 \\
x_4 &: \quad X2; && a_4 = -2.09059\ \text{min}^2/\mu\text{m}^2 \\
x_5 &: \quad Y2; && a_5 = -59.4658\ \text{min}^2/\mu\text{m}^2 \\
x_6 &: \quad Z2; && a_6 = -133.798\,\text{min}^2/\mu\text{m}^2
\end{aligned}$$

Note X-axes position error has the lowest contribution to the optical loss since those axes are parallel to the optical axis. Contrarily the Z-axes have the largest effects.

Data availability

Data will be made available on request.

References

Attia, M., Kops, L., 1979. Nonlinear thermoelastic behavior of structural joints—solution to a missing link for prediction of thermal deformation of machine tools. J. Manuf. Sci. Engenering.

Barber, J., 2016. Frictionally-Excited Thermoelastic Instability (TEI). University of Michigan, Online available under: http://www-personal.umich.edu/~jbarber/TEI.html, latest accessed at 15.

Beijen, M.A., Voorhoeve, R., Heertjes, M.F., Oomen, T., 2018. Experimental estimation of transmissibility matrices for industrial multi-axis vibration isolation systems. Mech. Syst. Signal Process. 107, 469–483.

Berline, N., Getzler, E., Vergne, M., 2003. Heat Kernels and Dirac Operators. Springer Science & Business Media.

Bernabé, S., Tekin, T., Sirbu, B., Charbonnier, J., Grosse, P., Seyfried, M., 2023. Packaging and test of photonic integrated circuits (PICs). Integr. Nanophotonics: Platf. Devices Appl. 1–52.

Blaser, P., Pavliček, F., Mori, K., Mayr, J., Weikert, S., Wegener, K., 2017. Adaptive learning control for thermal error compensation of 5-axis machine tools. J. Manuf. Syst. 44, 302–309.

Casazza, P.G., Kutyniok, G., 2012. Finite Frames: Theory and Applications. Springer Science & Business Media.

Chen, J., Yuan, J., Ni, J., 1996. Thermal error modelling for real-time error compensation. Int. J. Adv. Manuf. Technol. 12, 266–275.

Drebushchak, V., 2020. Thermal expansion of solids: review on theories. J. Therm. Anal. Calorim. 142 (2), 1097–1113.

Duffin, R.J., Schaeffer, A.C., 1952. A class of nonharmonic Fourier series. Trans. Amer. Math. Soc. 72 (2), 341–366.

Evers, E., De Jager, B., Oomen, T., 2018. Thermo-mechanical behavior in precision motion control: unified framework for fast and accurate FRF identification. In: IECON 2018-44th Annual Conference of the IEEE Industrial Electronics Society. IEEE, pp. 4618–4623.

Gao, G., Kuang, L., Liu, F., Xing, Y., Shi, Q., 2023. Modeling and parameter identification of a 3D measurement system based on redundant laser range sensors for industrial robots. Sensors 23 (4), http://dx.doi.org/10.3390/s23041913.

Jedrzejewski, J., Kwasny, W., Kowal, Z., Modrzycki, W., 2008. Precise model of HSC machining centre for aerospace parts machining. J. Mach. Eng. 8.

Jiao, Y., van der Tol, J., Pogoretskii, V., van Engelen, J., Kashi, A.A., Reniers, S., Wang, Y., Zhao, X., Yao, W., Liu, T., et al., 2020. Indium phosphide membrane nanophotonic integrated circuits on silicon. Phys. Status Solidi (a) 217 (3), 1900606.

Kim, B.-S., Song, Y.-C., Park, C.-H., 2011. Robust thermal error modeling and compensation for a nano level thermal drift in a high precision lathe. Int. J. Precis. Eng. Manuf. 12, 657–661.

Klamkin, J., Zhao, H., Song, B., Liu, Y., Isaac, B., Pinna, S., Sang, F., Coldren, L., 2018. Indium phosphide photonic integrated circuits: Technology and applications. In: 2018 IEEE BiCMOS and Compound Semiconductor Integrated Circuits and Technology Symposium. BCICTS, IEEE, pp. 8–13.

Lee, J.S., Carroll, L., Scarcella, C., Pavarelli, N., Menezo, S., Bernabé, S., Temporiti, E., O'Brien, P., 2016. Meeting the electrical, optical, and thermal design challenges of photonic-packaging. IEEE J. Sel. Top. Quantum Electron. 22 (6), 409–417.

Leijtens, X., Santos, R., Williams, K., 2020. High density multi-channel passively aligned optical probe for testing of photonic integrated circuits. IEEE Photonics J. 13 (1), 1–15.

Li, R., Zhao, Y., 2016. Dynamic error compensation for industrial robot based on thermal effect model. Measurement 88, 113–120. http://dx.doi.org/10.1016/j.measurement.2016.02.038.

Lubrano, E., Clavel, R., 2008. Thermal behavior of an ultra high-precision linear axis operating in industrial environment. In: REM 2008 9th International Workshop on Research and Education in Mechatronics. Schönenfeld & Ziegler, pp. 151–152.

Lubrano, E., Clavel, R., 2010. Thermal calibration of a 3 DOF ultra high-precision robot operating in industrial environment. In: 2010 IEEE International Conference on Robotics and Automation. IEEE, pp. 3692–3697.

Mallat, S., 2008. A Wavelet Tour of Signal Processing, Third Edition: The Sparse Way, third ed. Academic Press, Inc., USA.

Mandelli, L., Dankwart, C., Napoli, C., 2025. Motion stage precision prediction for photonic integrated circuit assembly. J. Intell. Manuf. 1–14.

Mayr, J., Blaser, P., Ryser, A., Hernandez-Becerro, P., 2018. An adaptive self-learning compensation approach for thermal errors on 5-axis machine tools handling an arbitrary set of sample rates. CIRP Ann 67 (1), 551–554.

Ngoc, H.V., Mayer, J., Bitar-Nehme, E., 2023. Deep learning to directly predict compensation values of thermally induced volumetric errors. Machines 11 (4), 496.

Pluta, Z., Hryniewicz, T., 2012. Thermal expansion of solids. J. Mod. Phys. 3 (08), 793–802.

Ramesh, R., Mannan, M., Poo, A., 2000. Error compensation in machine tools—a review: Part II: thermal errors. Int. J. Mach. Tools Manuf. 40 (9), 1257–1284.

Sigron, P., Aschwanden, I., Bambach, M., 2023. Compensation of geometric, backlash, and thermal drift errors using a universal industrial robot model. IEEE Trans. Autom. Sci. Eng..

Stejskal, T., Dovica, M., Demeč, P., Svetlík, J., Rajt'uková, V., 2017. Elimination of thermal drift in measuring the positioning accuracy of a three axis milling machine. Adv. Sci. Technol. Res. J. 11 (4).

Tan, K., Huang, S., Lee, T., 2003. Dynamic S-function for geometrical error compensation based on neural network approximations. Measurement 34 (2), 143–156.

Tu, Y.-H., Peng, C.-C., 2020. An ARMA-based digital twin for MEMS gyroscope drift dynamics modeling and real-time compensation. IEEE Sens. J. 21 (3), 2712–2724.

Vassilevich, D.V., 2003. Heat kernel expansion: user's manual. Phys. Rep. 388 (5–6), 279–360.

Vocetka, M., Bobovskỳ, Z., Babjak, J., Suder, J., Grushko, S., Mlotek, J., Krys, V., Hagara, M., 2021. Influence of drift on robot repeatability and its compensation. Appl. Sci. 11 (22), 10813.

Vogl, G.W., Rexford, A., Li, Z., Landers, R.G., Kinzel, E.C., Donmez, M.A., Chalfoun, J., 2023. Vision-based thermal drift monitoring method for machine tools. CIRP Ann 72 (1), 301–304.

Wang, Y., Jiao, Y., Williams, K., 2024. Scaling photonic integrated circuits with InP technology: A perspective. APL Photonics 9 (5).

Wu, L., Zhao, G., Yin, J., Feng, Z., 2021. A thermal drift compensation method for precision sensors considering historical temperature state. IEEE Trans. Ind. Electron. 68 (12), 12821–12829. http://dx.doi.org/10.1109/TIE.2020.3044777.

Yang, H., Ni, J., 2003. Dynamic modeling for machine tool thermal error compensation. J. Manuf. Sci. Eng. 125 (2), 245–254.

Yang, S., Zhang, J.-Y., Yang, Y.-Y., Huang, J.-Y., Bai, Y.-R., Zhang, Y., Lin, X.-C., 2019. Automatic compensation of thermal drift of laser beam through thermal balancing based on different linear expansions of metals. Results Phys. 13, 102201.

Zagrodzki, P., Lam, K.B., Al Bahkali, E., Barber, J.R., 2001. Nonlinear transient behavior of a sliding system with frictionally excited thermoelastic instability. J. Tribol. 123 (4), 699–708. http://dx.doi.org/10.1115/1.1353180.